



Published in final edited form as:

*Science*. 2017 February 24; 355(6327): 831–833. doi:10.1126/science.aaf4901.

## The cytotoxic *Staphylococcus aureus* PSM $\alpha$ 3 reveals a cross- $\alpha$ amyloid-like fibril

Einav Tayeb-Fligelman<sup>#1</sup>, Orly Tabachnikov<sup>#1</sup>, Asher Moshe<sup>#1</sup>, Orit Goldshmidt-Tran<sup>1</sup>, Michael R. Sawaya<sup>2</sup>, Nicolas Coquelle<sup>3</sup>, Jacques-Philippe Colletier<sup>3</sup>, and Meytal Landau<sup>1,†</sup>

<sup>1</sup>Department of Biology, Technion-Israel Institute of Technology, Haifa 3200003, Israel

<sup>2</sup>Department of Biological Chemistry, Department of Chemistry and Biochemistry, and Howard Hughes Medical Institute, University of California at Los Angeles, Los Angeles, California CA 9009590095, USA.

<sup>3</sup>Université Grenoble Alpes, CNRS and CEA, and IBS, Grenoble 38044, France

# These authors contributed equally to this work.

### Abstract

Amyloids are ordered protein aggregates, found in all kingdoms of life, and are involved in aggregation diseases as well as in physiological activities. In microbes, functional amyloids are often key virulence determinants, yet the structural basis for their activity remains elusive. We determined the fibril structure and function of the highly toxic, 22-residue phenol-soluble modulins  $\alpha$ 3 (PSM $\alpha$ 3) peptide secreted by *Staphylococcus aureus*. PSM $\alpha$ 3 formed elongated fibrils that shared the morphological and tinctorial characteristics of canonical cross- $\beta$  eukaryotic amyloids. However, the crystal structure of full-length PSM $\alpha$ 3, solved de novo at 1.45 angstrom resolution, revealed a distinctive “cross- $\alpha$ ” amyloid-like architecture, in which amphipathic  $\alpha$ -helices stacked perpendicular to the fibril axis into tight self-associating sheets. The cross- $\alpha$  fibrillation of PSM $\alpha$ 3 facilitated cytotoxicity, suggesting that this assembly mode underlies function in *Staphylococcus aureus*.

### One Sentence Summary

Fibrillation-dependent cytotoxicity of PSM $\alpha$ 3 functional amyloid is encoded by a cross- $\alpha$  architecture.

---

Amyloids are structured protein aggregates that encompass a variety of structures, ranging from small soluble oligomers to plaques of insoluble fibrils. Amyloids are most notorious for their involvement in human neurodegenerative diseases (e.g., Alzheimer’s and Parkinson’s diseases) (1). Insights into amyloid structures were long challenged by their polymorphic and partially disordered nature (2, 3), but advances in x-ray and electron micro-crystallography [e.g., (3–6)], cryo-electron microscopy [e.g., (7, 8)] and solid-state nuclear magnetic resonance (NMR) spectroscopy [e.g., (2, 9–12)] have substantially furthered the understanding of eukaryotic disease-associated amyloid properties and notable stability.

---

<sup>†</sup>Corresponding author. mlandau@technion.ac.il.

Eukaryotic amyloids share a common structural feature, namely, the cross- $\beta$  spine, in which individual  $\beta$ -strands run perpendicular to the fibril axis (13).

In contrast to disease-associated amyloids, functional amyloids, evident mostly in microbes, participate in diverse activities that benefit the producing organism (14–16). Thus far, structural knowledge of microbial amyloids has been lacking, as have been the possible differences between functional and disease-associated amyloids (17, 18). Functional amyloids were recently suggested to play a role in the pathogenicity of *Staphylococcus aureus*, a prominent cause of aggressive infections and an emerging public-health concern (19, 20). These amyloids are formed by several members of a family of secreted virulent peptides called phenol-soluble modulins (PSMs). PSMs stimulate inflammatory responses, lyse human cells, and contribute to biofilm structuring (20, 21). High expression of PSM $\alpha$ s is linked to the virulence potential of methicillin-resistant *S. aureus* (MRSA) (22). Amyloid fibrillation of some PSMs promote biofilm stability (20), yet the role of the amyloid state in other PSM activities is unclear.

The 22-residue peptide PSM $\alpha$ 3 is the most cytotoxic and lytic member of the PSM family (21, 23). PSM $\alpha$ 3 forms amphipathic helices (21, 23), as shown by solution NMR (24). Yet the helix alone is not sufficient to achieve biological activities (21). We found that PSM $\alpha$ 3 formed elongated and un-branched fibrils (Fig. 1A), which bound the amyloid-indicator dye Thioflavin T, generating high levels of fluorescence emission and a characteristic amyloid-fibrillation curve (Fig. 1B and fig. S1). Whereas previously characterized amyloid proteins convert into  $\beta$ -pleated structures during fibril formation (1), we found that PSM $\alpha$ 3 maintained its  $\alpha$ -helical conformation, both in solution and in the fibrils (fig. S2 and table S1). The x-ray diffraction pattern of PSM $\alpha$ 3 indicated that the fibrils were indeed built from the stacking of  $\alpha$ -helices (fig. S3 and supplementary methods).

To understand the atomic basis of these  $\alpha$ -helical fibrils, we solved the micro-crystallographic fibril structure of full-length PSM $\alpha$ 3 at 1.45 Å resolution (Fig. 1 and table S2), using de novo phasing methods (25). The structure revealed amphipathic  $\alpha$ -helices positioned perpendicular to the fibril axis, which stacked into sheets that ran parallel to the fibril axis and mated through the hydrophobic faces of the helix (Fig. 1, D and E, and figs. S4 and S5). This “cross- $\alpha$ ” amyloid-like fibril is has not been observed previously in structures of eukaryotic amyloids solved to date. The structural characteristics of PSM $\alpha$ 3 fibrils were nevertheless reminiscent of those displayed by cross- $\beta$  fibrils, which also feature in-register stacking of a structural element into sheets, that mate through a dry interface (Fig. 2 and fig. S6). The chemical properties governing cross- $\alpha$  fibril stability, i.e., buried surface area and shape complementarity between sheets, resembled those of cross- $\beta$  structures (figs. S4 to S7 and table S3). These structural characteristics suggested that the binding of the amyloid-indicator dye Thioflavin T to PSM $\alpha$ 3 fibrils (Fig 1B and figs. S1 and S8) probably occurs via cavities running parallel to the fibril axis. These cavities bear the characteristics of repeating structures that exist mainly in  $\beta$ -rich amyloid fibrils, but also within some  $\alpha$ -helical rich environments (26, 27). Thioflavin T binding to these cavities is often mediated by aromatic side chains (26), which were indeed abundant in the PSM $\alpha$ 3 sequence (Fig. 1C). Overall, PSM $\alpha$ 3 fibrils not only shared the morphological and tinctorial properties of amyloid fibrils, but also exhibited a cross- $\alpha$  architecture reminiscent of cross- $\beta$  amyloids,

notwithstanding the fundamental difference that the fibrils were formed of  $\alpha$ -helices rather than  $\beta$ -strands (Fig. 2).

To explore whether fibrillation plays a role in PSM $\alpha$ 3 cytotoxicity, we performed mutagenesis analysis to identify PSM $\alpha$ 3 mutants that do not fibrillate, and discovered F3A and the K9P/F11P double mutant (A, Ala; F, Phe; K, Lys; P, Pro) (figs. S8 and S9). The two mutants displayed much lower T-cell cytotoxicity compared to wild-type PSM $\alpha$ 3 (Fig. 3A). In contrast, the G16A mutant (G, Gly), which forms fibrils recognized by Thioflavin T, thus serving as control, was highly cytotoxic (Fig. 3A and figs. S8 and S9). Whereas the K9P/F11P double mutant was mostly unstructured in solution, both G16A and F3A mutants maintained  $\alpha$ -helical conformation (fig. S8), reinforcing the notion that helical conformation alone is not sufficient for cytotoxicity. Furthermore, the addition of a biocompatible surfactant maintained  $\alpha$ -helicity, but diminished fibrillation and abrogated PSM $\alpha$ 3 toxicity (Fig. 3B and figs. S8 and S10). The same pattern of fibrillation-dependent cytotoxicity was recorded also against human embryonic kidney 293 (HEK293) cells (fig. S11), suggesting that the lytic activity of PSM $\alpha$ 3 fibrils is not cell-specific. It is possible that this cytotoxicity stems from self-assembly of helices that form large “carpets” of amphipathic sheets (fig. S6) on the membrane surface, triggering its deformation (28). The exact conformation that contributes to amyloid toxicity is still under debate. In some human disease-associated amyloids, the toxic entity has been attributed to a prefibrillar conformation, whereas the mature  $\beta$ -rich fibrils detoxify the amyloid (29). Several eukaryotic amyloid proteins contain  $\alpha$ -helices in their monomeric or prefibrillar intermediate states [e.g., (30)], or even in the fibril state [e.g., (27)], suggesting a link to the cytotoxicity induced by the fibrillation of PSM $\alpha$ 3 into purely helical species.

In this work, we have demonstrated, at atomic resolution, that cross- $\alpha$  fibrillation of PSM $\alpha$ 3 into amyloid-like fibrils is required for cytotoxicity and suggest a key role for cross- $\alpha$  fibrils in *S. aureus* pathogenicity. PSM $\alpha$ 3 is thus a functional amyloid, displaying architecture and properties similar to those of eukaryotic cross- $\beta$  fibrils, but differs in its secondary structure elements. Among the large variety of super-helical assemblies found in nature,  $\alpha$ -helices that stack perpendicular to the fibril axis are rare; the few examples include de novo-designed amphiphilic peptides (28, 31, 32) and ultra-stable proteins of multiple tandem copies of a helix-loop-helix unit (33) that bear no sequence relationship to PSM $\alpha$ 3. We thus conclude that the cross- $\alpha$  architecture is robust and compatible with divergent sequences. It remains to be seen whether PSM $\alpha$ 3 is a unique example of a natural cross- $\alpha$  fibril. The crystal structure of the PSM $\alpha$ 3 should contribute to research on protein aggregation, biomaterial design, and antibacterial therapeutics.

## Supplementary Material

Refer to Web version on PubMed Central for supplementary material.

## Acknowledgments

We are grateful to D. Eisenberg for discussions and for his insight. We acknowledge S. Fleishman, R. Diskin, and N. Ben-Tal for helpful comments. M.L. thanks the U.S.-Israel Binational Science Foundation (BSF) (grant no. 2013254); Alon Fellowships for Outstanding Young Researchers by the Israeli Council for Higher Education;

David and Inez Mayers Career Advancement Chair in Life Sciences; the J. and A. Taub Biological Research Fund; the I-CORE Program of the Planning and Budgeting Committee and the Israel Science Foundation, Center of Excellence in Integrated Structural Cell Biology (grant no. 1775/12); the Support for Training and Career Development of Researchers (Marie Curie Career Integration Grants), Seventh Framework Program (FP7) of the European Commission, Single Beneficiary (grant no. 334260), DFG: Deutsch-IsraelischeProjektkooperation (DIP) (grant no. LA 3655/1-1), and BioStruct-X funded by FP7. J.-P.C. gratefully acknowledges the support of the France Alzheimer Foundation (FA-AAP-2013-65-101349) and the Agence Nationale de la Recherche (ANR-12-BS07-0008-03). M.R.S. acknowledges support from the Howard Hughes Medical Institute. We acknowledge Y. Pazy-Benhar, H. Dvir, and D. Hiya (Technion Center for Structural Biology). We thank M. Baskin (Technion) for support with CD experiments. This work is based on research conducted at the ID13 and ID23-EH2 beamlines at the European Synchrotron Radiation Facility (ESRF), and at the Northeastern Collaborative Access Team beamlines funded by the National Institute of General Medical Sciences from the National Institutes of Health (P41 GM103403). The Pilatus 6M detector on 24-ID-C beamline is funded by a NIH-ORIP HEI grant (S10 RR029205). This research used resources of the Advanced Photon Source, a U.S. Department of Energy (DOE) Office of Science User Facility operated for the DOE Office of Science by Argonne National Laboratory under Contract no. DE-AC02-06CH11357. We appreciatively acknowledge ESRF and APS for beamtime and assistance during data collection. Coordinates and structure factors for the x-ray crystal structures of PSM $\alpha$ 3 have been deposited in the Protein Data Bank (PDB) with accession code 5155.

## References and Notes:

1. Eisenberg D, Jucker M, The amyloid state of proteins in human diseases. *Cell* 148, 1188–1203 (2012). [PubMed: 22424229]
2. Paravastu AK, Leapman RD, Yau WM, Tycko R, Molecular structural basis for polymorphism in Alzheimer's  $\beta$ -amyloid fibrils. *Proc. Natl. Acad. Sci. U. S. A* 105, 18349–18354 (2008). [PubMed: 19015532]
3. Colletier J-P, Laganowsky A, Landau M, Zhao M, Soriaga AB, Goldschmidt L, Flot D, Cascio D, Sawaya MR, Eisenberg D, Molecular basis for amyloid-beta polymorphism. *Proc. Natl. Acad. Sci. U.S.A* 108, 16938–16943 (2011). [PubMed: 21949245]
4. Nelson R, Sawaya MR, Balbirnie M, Madsen AO, Riek C, Grothe R, Eisenberg D, Structure of the cross-beta spine of amyloid-like fibrils. *Nature* 435, 773–778 (2005). [PubMed: 15944695]
5. Sawaya MR, Sambashivan S, Nelson R, Ivanova MI, Sievers SA, Apostol MI, Thompson MJ, Balbirnie M, Wiltzius JJ, McFarlane HT, Madsen AO, Riek C, Eisenberg D, Atomic structures of amyloid cross-beta spines reveal varied steric zippers. *Nature* 447, 453–457 (2007). [PubMed: 17468747]
6. Rodriguez JA, Ivanova MI, Sawaya MR, Cascio D, Reyes FE, Shi D, Sangwan S, Guenther EL, Johnson LM, Zhang M, Jiang L, Arbing MA, Nannenga BL, Hattne J, Whitelegge J, Brewster AS, Messerschmidt M, Boutet S, Sauter NK, Gonen T, Eisenberg DS, Structure of the toxic core of alpha-synuclein from invisible crystals. *Nature* 525, 486–490 (2015). [PubMed: 26352473]
7. Chen SW, Drakulic S, Deas E, Ouberaï M, Aprile FA, Arranz R, Ness S, Roodveldt C, Williams T, De-Genst EJ, Klenerman D, Wood NW, Knowles TP, Alfonso C, Rivas G, Abramov AY, Valpuesta JM, Dobson CM, Cremades N, Structural characterization of toxic oligomers that are kinetically trapped during alpha-synuclein fibril formation. *Proc. Natl. Acad. Sci. U.S.A* 112, E1994–2003 (2015). [PubMed: 25855634]
8. Schmidt M, Rohou A, Lasker K, Yadav JK, Schiene-Fischer C, Fandrich M, Grigorieff N, Peptide dimer structure in an Abeta(1–42) fibril visualized with cryo-EM. *Proc. Natl. Acad. Sci. U.S.A* 112, 11858–11863 (2015). [PubMed: 26351699]
9. Xiao Y, Ma B, McElheny D, Parthasarathy S, Long F, Hoshi M, Nussinov R, Ishii Y, Abeta(1–42) fibril structure illuminates self-recognition and replication of amyloid in Alzheimer's disease. *Nat. Struct. Mol. Biol* 22, 499–505 (2015). [PubMed: 25938662]
10. Van Melckebeke H, Wasmer C, Lange A, Ab E, Loquet A, Bockmann A, Meier BH, Atomic-resolution three-dimensional structure of HET-s(218–289) amyloid fibrils by solid-state NMR spectroscopy. *J. Am. Chem. Soc* 132, 13765–13775 (2010). [PubMed: 20828131]
11. Colvin MT, Silvers R, Ni QZ, Can TV, Sergeyev I, Rosay M, Donovan KJ, Michael B, Wall J, Linse S, Griffin RG, Atomic Resolution Structure of Monomorphic Abeta42 Amyloid Fibrils. *J. Am. Chem. Soc* 138, 9663–9674 (2016). [PubMed: 27355699]

12. Walti MA, Ravotti F, Arai H, Glabe CG, Wall JS, Bockmann A, Guntert P, Meier BH, Riek R, Atomic-resolution structure of a disease-relevant A $\beta$ (1–42) amyloid fibril. *Proc. Natl. Acad. Sci. U.S.A* 113, E4976–4984 (2016). [PubMed: 27469165]
13. Sunde M, Serpell LC, Bartlam M, Fraser PE, Pepys MB, Blake CC, Common core structure of amyloid fibrils by synchrotron X-ray diffraction. *J. Mol. Biol* 273, 729–739 (1997). [PubMed: 9356260]
14. Maji SK, Perrin MH, Sawaya MR, Jessberger S, Vadodaria K, Rissman RA, Singru PS, Nilsson KP, Simon R, Schubert D, Eisenberg D, Rivier J, Sawchenko P, Vale W, Riek R, Functional amyloids as natural storage of peptide hormones in pituitary secretory granules. *Science* 325, 328–332 (2009). [PubMed: 19541956]
15. Chapman MR, Robinson LS, Pinkner JS, Roth R, Heuser J, Hammar M, Normark S, Hultgren SJ, Role of *Escherichia coli* curli operons in directing amyloid fiber formation. *Science* 295, 851–855 (2002). [PubMed: 11823641]
16. DePas WH, Chapman MR, Microbial manipulation of the amyloid fold. *Res. Microbiol* 163, 592–606 (2012). [PubMed: 23108148]
17. Schubeis T, Yuan P, Ahmed M, Nagaraj M, van Rossum BJ, Ritter C, Untangling a Repetitive Amyloid Sequence: Correlating Biofilm-Derived and Segmentally Labeled Curli Fimbriae by Solid-State NMR Spectroscopy. *Angew. Chem. Int. Ed. Engl* 54, 14669–14672 (2015). [PubMed: 26474178]
18. Shewmaker F, McGlinchey RP, Thurber KR, McPhie P, Dyda F, Tycko R, Wickner RB, The functional curli amyloid is not based on in-register parallel beta-sheet structure. *J. Biol. Chem* 284, 25065–25076 (2009). [PubMed: 19574225]
19. Schwartz K, Ganesan M, Payne DE, Solomon MJ, Boles BR, Extracellular DNA facilitates the formation of functional amyloids in *Staphylococcus aureus* biofilms. *Mol. Microbiol* 99, 123–134 (2016). [PubMed: 26365835]
20. Schwartz K, Syed AK, Stephenson RE, Rickard AH, Boles BR, Functional amyloids composed of phenol soluble modulins stabilize *Staphylococcus aureus* biofilms. *PLoS Pathog* 8, e1002744 (2012). [PubMed: 22685403]
21. Cheung GY, Kretschmer D, Queck SY, Joo HS, Wang R, Duong AC, Nguyen TH, Bach TH, Porter AR, DeLeo FR, Peschel A, Otto M, Insight into structure-function relationship in phenol-soluble modulins using an alanine screen of the phenol-soluble modulin (PSM) alpha3 peptide. *FASEB J* 28, 153–161 (2014). [PubMed: 24008753]
22. Wang R, Braughton KR, Kretschmer D, Bach TH, Queck SY, Li M, Kennedy AD, Dorward DW, Klebanoff SJ, Peschel A, DeLeo FR, Otto M, Identification of novel cytolytic peptides as key virulence determinants for community-associated MRSA. *Nat. Med* 13, 1510–1514 (2007). [PubMed: 17994102]
23. Laabei M, Jamieson WD, Yang Y, van den Elsen J, Jenkins AT, Investigating the lytic activity and structural properties of *Staphylococcus aureus* phenol soluble modulin (PSM) peptide toxins. *Biochim. Biophys. Acta* 1838, 3153–3161 (2014). [PubMed: 25194683]
24. Towle KM, Lohans CT, Miskolzie M, Acedo JZ, van Belkum MJ, Vederas JC, Solution Structures of Phenol-Soluble Modulins alpha1, alpha3, and beta2, Virulence Factors from *Staphylococcus aureus*. *Biochemistry* 55, 4798–4806 (2016). [PubMed: 27525453]
25. Rodriguez DD, Grosse C, Himmel S, Gonzalez C, de Ilarduya IM, Becker S, Sheldrick GM, Uson I, Crystallographic ab initio protein structure solution below atomic resolution. *Nat. Methods* 6, 651–653 (2009). [PubMed: 19684596]
26. Groenning M, Olsen L, van de Weert M, Flink JM, Frokjaer S, Jorgensen FS, Study on the binding of Thioflavin T to beta-sheet-rich and non-beta-sheet cavities. *J. Struct. Biol* 158, 358–369 (2007). [PubMed: 17289401]
27. Bousset L, Thomson NH, Radford SE, Melki R, The yeast prion Ure2p retains its native alpha-helical conformation upon assembly into protein fibrils in vitro. *EMBO J* 21, 2903–2911 (2002). [PubMed: 12065404]
28. Taylor KS, Lou MZ, Chin TM, Yang NC, Garavito RM, A novel, multilayer structure of a helical peptide. *Protein Sci* 5, 414–421 (1996). [PubMed: 8868477]

29. Stefani M, Structural features and cytotoxicity of amyloid oligomers: implications in Alzheimer's disease and other diseases with amyloid deposits. *Prog. Neurobiol* 99, 226–245 (2012). [PubMed: 22450705]
30. Ghosh D, Singh PK, Sahay S, Jha NN, Jacob RS, Sen S, Kumar A, Riek R, Maji SK, Structure based aggregation studies reveal the presence of helix-rich intermediate during alpha-Synuclein aggregation. *Sci. Rep* 5, 9228 (2015). [PubMed: 25784353]
31. Prive GG, Anderson DH, Wesson L, Cascio D, Eisenberg D, Packed protein bilayers in the 0.90 Å resolution structure of a designed alpha helical bundle. *Protein Sci* 8, 1400–1409 (1999). [PubMed: 10422828]
32. Mondal S, Adler-Abramovich L, Lampel A, Bram Y, Lipstman S, Gazit E, Formation of functional super-helical assemblies by constrained single heptad repeat. *Nat. Commun* 6, 8615 (2015). [PubMed: 26468599]
33. Brunette TJ, Parmeggiani F, Huang PS, Bhabha G, Ekiert DC, Tsutakawa SE, Hura GL, Tainer JA, Baker D, Exploring the repeat protein universe through computational protein design. *Nature* 528, 580–584 (2015). [PubMed: 26675729]
34. Rogers DR, Screening for the amyloid with the thioflavin-T fluorescent method. *Am. J. Clin. Pathol* 44, 59–61 (1965). [PubMed: 14314221]
35. Anthis NJ, Clore GM, Sequence-specific determination of protein and peptide concentrations by absorbance at 205 nm. *Protein Sci* 22, 851–858 (2013). [PubMed: 23526461]
36. Bohm G, Muhr R, Jaenicke R, Quantitative analysis of protein far UV circular dichroism spectra by neural networks. *Protein Eng* 5, 191–195 (1992). [PubMed: 1409538]
37. Micsonai A, Wien F, Kernya L, Lee YH, Goto Y, Refregiers M, Kardos J, Accurate secondary structure prediction and fold recognition for circular dichroism spectroscopy. *Proc. Natl. Acad. Sci. U.S.A* 112, E3095–3103 (2015). [PubMed: 26038575]
38. Hammersley AP, Svensson SO, Hanfland M, Fitch AN, Häusermann D, Two-Dimensional Detector Software: From Real Detector to Idealised Image or Two-Theta Scan. *High Pressure Res* 14, 235–248 (1996).
39. Favre-Nicolin V, Cerny R, FOX, 'free objects for crystallography': a modular approach to ab initio structure determination from powder diffraction. *J. Appl. Cryst* 35, (2002).
40. Bortolotti M, Lonardelli I, ReX.Cell: a user-friendly program for powder diffraction indexing. *J. Appl. Cryst* 46, 259–261 (2013).
41. Boultif A, Louër D, Powder pattern indexing with the dichotomy method. *J. Appl. Cryst* 37, 724–731 (2004).
42. Le Bail A, Monte Carlo indexing with McMaille. *Powder Diffr* 19, 249–254 (2004).
43. Kabsch W, XDS. *Acta Crystallogr. D Biol. Crystallogr* 66, 125–132 (2010). [PubMed: 20124692]
44. Holton J, XANES measurements of the rate of radiation damage to selenomethionine side chains. *J. Synchrotron Radiat* 14, 51–72 (2007). [PubMed: 17211072]
45. Weiss M, Global indicators of X-ray data quality. *J. Appl. Cryst* 34, 130–135 (2001).
46. Adams PD, Afonine PV, Bunkoczi G, Chen VB, Davis IW, Echols N, Headd JJ, Hung LW, Kapral GJ, Grosse-Kunstleve RW, McCoy AJ, Moriarty NW, Oeffner R, Read RJ, Richardson DC, Richardson JS, Terwilliger TC, Zwart PH, PHENIX: a comprehensive Python-based system for macromolecular structure solution. *Acta Crystallogr. D Biol. Crystallogr* 66, 213–221 (2010). [PubMed: 20124702]
47. Terwilliger TC, Grosse-Kunstleve RW, Afonine PV, Moriarty NW, Zwart PH, Hung LW, Read RJ, Adams PD, Iterative model building, structure refinement and density modification with the PHENIX AutoBuild wizard. *Acta Crystallogr. D Biol. Crystallogr* 64, 61–69 (2008). [PubMed: 18094468]
48. Murshudov GN, Vagin AA, Dodson EJ, Refinement of macromolecular structures by the maximum-likelihood method. *Acta Crystallogr. D Biol. Crystallogr* 53, 240–255 (1997). [PubMed: 15299926]
49. Emsley P, Cowtan K, Coot: model-building tools for molecular graphics. *Acta Crystallogr. D Biol. Crystallogr* 60, 2126–2132 (2004). [PubMed: 15572765]



50. Pettersen EF, Goddard TD, Huang CC, Couch GS, Greenblatt DM, Meng EC, Ferrin TE, UCSF Chimera—a visualization system for exploratory research and analysis. *J. Comput. Chem* 25, 1605–1612 (2004). [PubMed: 15264254]
51. Kyte J, Doolittle RF, A simple method for displaying the hydropathic character of a protein. *J. Mol. Biol* 157, 105–132 (1982). [PubMed: 7108955]
52. Petkova AT, Yau WM, Tycko R, Experimental constraints on quaternary structure in Alzheimer's beta-amyloid fibrils. *Biochemistry* 45, 498–512 (2006). [PubMed: 16401079]
53. Schrodinger LLC, The PyMOL Molecular Graphics System, Version 1.8 (2015).
54. Lawrence MC, Colman PM, Shape complementarity at protein/protein interfaces. *J. Mol. Biol* 234, 946–950 (1993). [PubMed: 8263940]
55. Lee B, Richards FM, The interpretation of protein structures: estimation of static accessibility. *J. Mol. Biol* 55, 379–400 (1971). [PubMed: 5551392]
56. Saff EB, Kuijlaars ABJ, Distributing many points on a sphere. *Math. Intelligencer* 19, 5–11 (1997).
57. Winn MD, Ballard CC, Cowtan KD, Dodson EJ, Emsley P, Evans PR, Keegan RM, Krissinel EB, Leslie AG, McCoy A, McNicholas SJ, Murshudov GN, Pannu NS, Potterton EA, Powell HR, Read RJ, Vagin A, Wilson KS, Overview of the CCP4 suite and current developments. *Acta Crystallogr. D Biol. Crystallogr* 67, 235–242 (2011). [PubMed: 21460441]
58. Altschul SF, Gish W, Miller W, Myers EW, Lipman DJ, Basic local alignment search tool. *J. Mol. Biol* 215, 403–410 (1990). [PubMed: 2231712]
59. Remmert M, Biegert A, Hauser A, Soding J, HHblits: lightning-fast iterative protein sequence searching by HMM-HMM alignment. *Nat. Methods* 9, 173–175 (2012).
60. Holm L, Rosenstrom P, Dali server: conservation mapping in 3D. *Nucleic Acids Res* 38, W545–549 (2010). [PubMed: 20457744]
61. Patterson WR, Anderson DH, DeGrado WF, Cascio D, Eisenberg D, Centrosymmetric bilayers in the 0.75 Å resolution structure of a designed alpha-helical peptide, D,L-Alpha-1. *Protein Sci* 8, 1410–1422 (1999). [PubMed: 10422829]
62. Hayouka Z, Thomas NC, Mortenson DE, Satyshur KA, Weisblum B, Forest KT, Gellman SH, Quasiracemate Crystal Structures of Magainin 2 Derivatives Support the Functional Significance of the Phenylalanine Zipper Motif. *J. Am. Chem. Soc* 137, 11884–11887 (2015). [PubMed: 26369301]
63. Miyazawa T, Blout ER, The Infrared Spectra of Polypeptides in Various Conformations: Amide I and II Bands. *J. Am. Chem. Soc* 83, 712–719 (1961).
64. Yang H, Yang S, Kong J, Dong A, Yu S, Obtaining information about protein secondary structures in aqueous solution using Fourier transform IR spectroscopy. *Nat. Protocols* 10, 382–396 (2015). [PubMed: 25654756]
65. Haris PI, Chapman D, The conformational analysis of peptides using Fourier transform IR spectroscopy. *Biopolymers* 37, 251–263 (1995). [PubMed: 7540054]
66. Cabiaux V, Brasseur R, Wattiez R, Falmagne P, Ruyschaert JM, Goormaghtigh E, Secondary structure of diphtheria toxin and its fragments interacting with acidic liposomes studied by polarized infrared spectroscopy. *J. Biol. Chem* 264, 4928–4938 (1989). [PubMed: 2925676]
67. Chen VB, Arendall WB, 3rd, Headd JJ, Keedy DA, Immormino RM, Kapral GJ, Murray LW, Richardson JS, Richardson DC, MolProbity: all-atom structure validation for macromolecular crystallography. *Acta Crystallogr. D Biol. Crystallogr* 66, 12–21 (2010). [PubMed: 20057044]
68. Diederichs K, Karplus PA, Improved R-factors for diffraction data analysis in macromolecular crystallography. *Nat. Struct. Biol* 4, 269–275 (1997). [PubMed: 9095194]
69. Karplus PA, Diederichs K, Linking crystallographic model and data quality. *Science* 336, 1030–1033 (2012). [PubMed: 22628654]
70. Brunger AT, Free R value: a novel statistical quantity for assessing the accuracy of crystal structures. *Nature* 355, 472–475 (1992). [PubMed: 18481394]

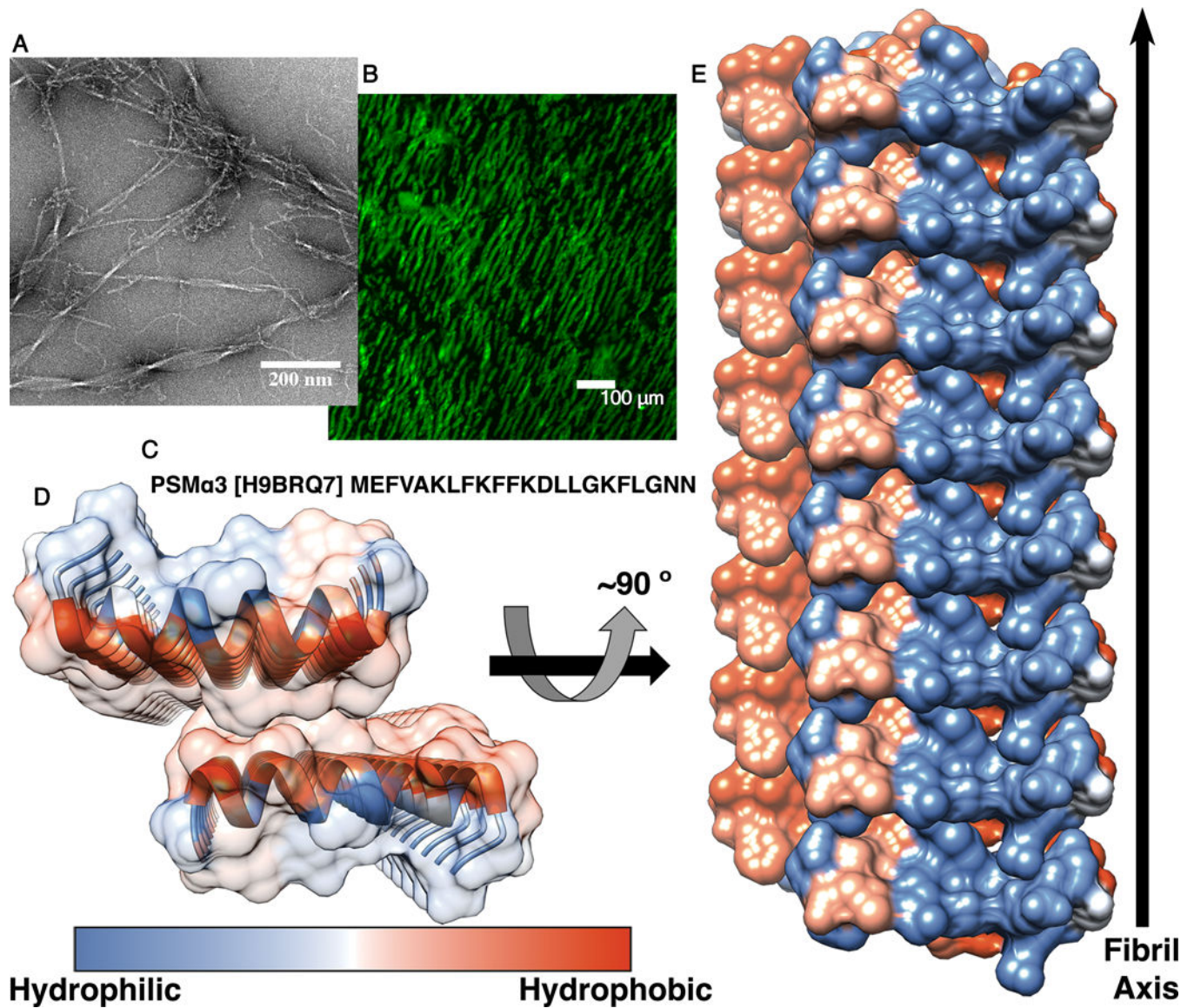


**Fig. 1. The cross- $\alpha$  amyloid-like fibril of the full-length PSM $\alpha$ 3.**

(A) An electron micrograph of PSM $\alpha$ 3 fibrils. (B) Fluorescence microscopy images of Thioflavin T stained PSM $\alpha$ 3 fibrils. (C) The sequence of *S. aureus* PSM $\alpha$ 3 (UniProt accession number is indicated in brackets). (D and E) The crystal structure of PSM $\alpha$ 3 at 1.45 Å resolution, colored according to hydrophobicity (a colored scale bar is shown). (D) A view down the fibril axis. PSM $\alpha$ 3 forms parallel  $\alpha$ -helical stacks, viewed as ribbons along with a semitransparent surface representation. Facing helical sheets are oriented head to tail. (E) A view perpendicular to the fibril axis. The helices, shown in surface representation, run horizontally. Eight layers of  $\alpha$ -helices forming the cross- $\alpha$  structure are depicted. Theoretically, fibrils can contain tens of thousands of layers. The  $\alpha$ -helical sheets interact via their hydrophobic face, creating a tight interface. The higher order packing of the crystal structure shows continuous rows of sheets that generate alternating hydrophobic and hydrophilic interfaces (fig. S6A). Single-letter abbreviations for the amino acid residues are



as follows: A, Ala; D, Asp; E, Glu; F, Phe; G, Gly; K, Lys; L, Leu; M, Met; N, Asn; and V, Val.

Author Manuscript

Author Manuscript

Author Manuscript

Author Manuscript

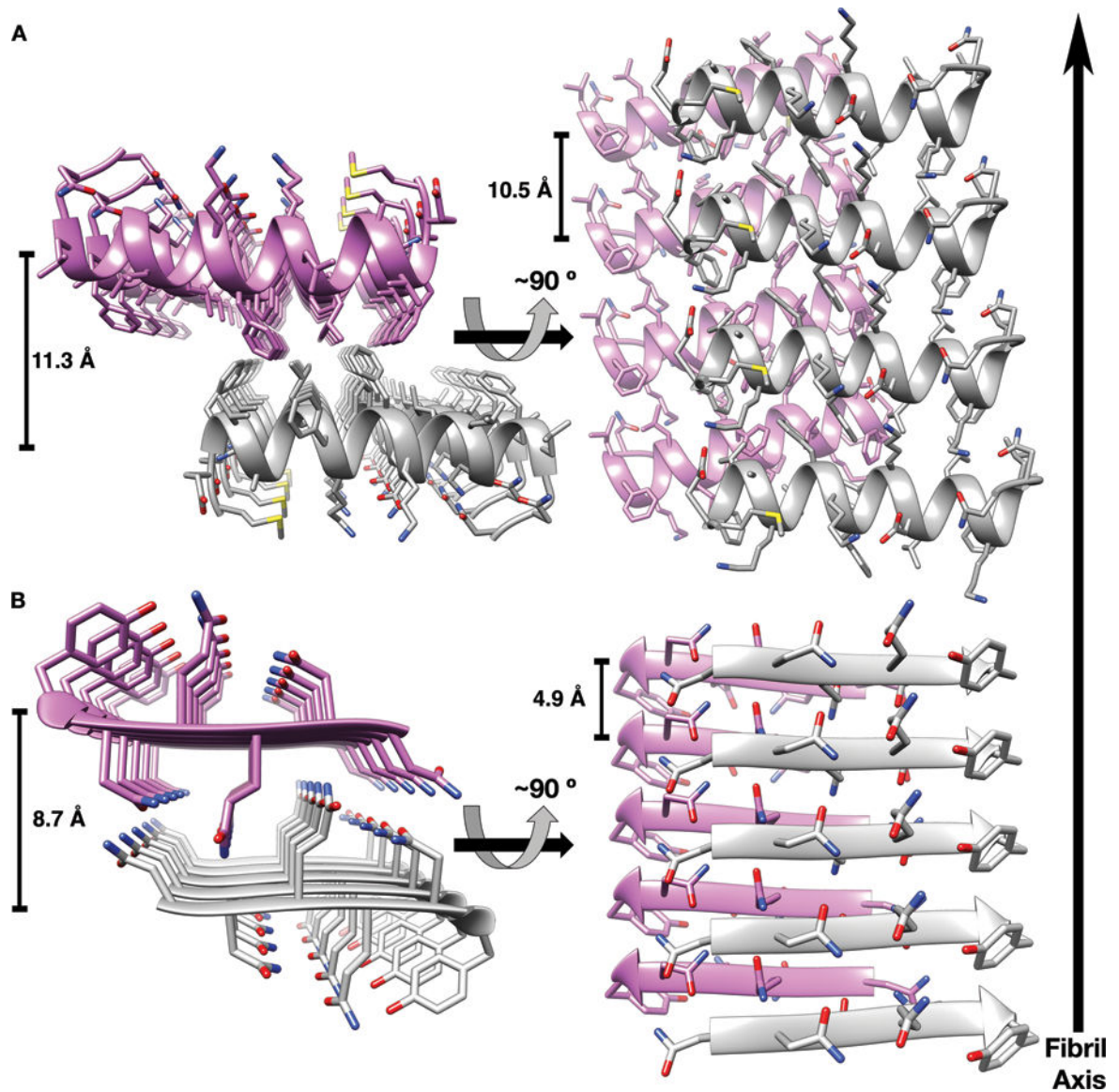


**Fig. 2. PSM $\alpha$ 3 cross- $\alpha$  fibril is reminiscent of amyloid cross- $\beta$  structure.**

(A) The crystal structure of PSM $\alpha$ 3. Two mating  $\alpha$ -helical sheets are shown. (B) The steric zipper structure of the NNQQNY N, Asn; Q, Gln; Y, Tyr) segment from yeast prion Sup35 (4) (PDB code 1YJO) forms the cross- $\beta$  spine of amyloid-like fibrils. The two mating  $\beta$ -sheets are composed of parallel  $\beta$ -strands. In both PSM $\alpha$ 3 (A) and NNQQNY (B) structures, side-chains protruding from the two sheets intermesh to form a dry, tightly self-complementing interface. The two sheets, in purple and gray, are shown as ribbons, with side chain as sticks. Heteroatoms are colored by atom type (nitrogen in blue, oxygen in red, and sulfur in yellow). In the left panels, the view looks down the fibril axis, and in the right panels, the view is roughly perpendicular to the fibril axis. The  $\alpha$ -helices (A) and  $\beta$ -strands (B) run horizontally. Distances between mating sheets and between strands along the sheet are displayed (table S3).

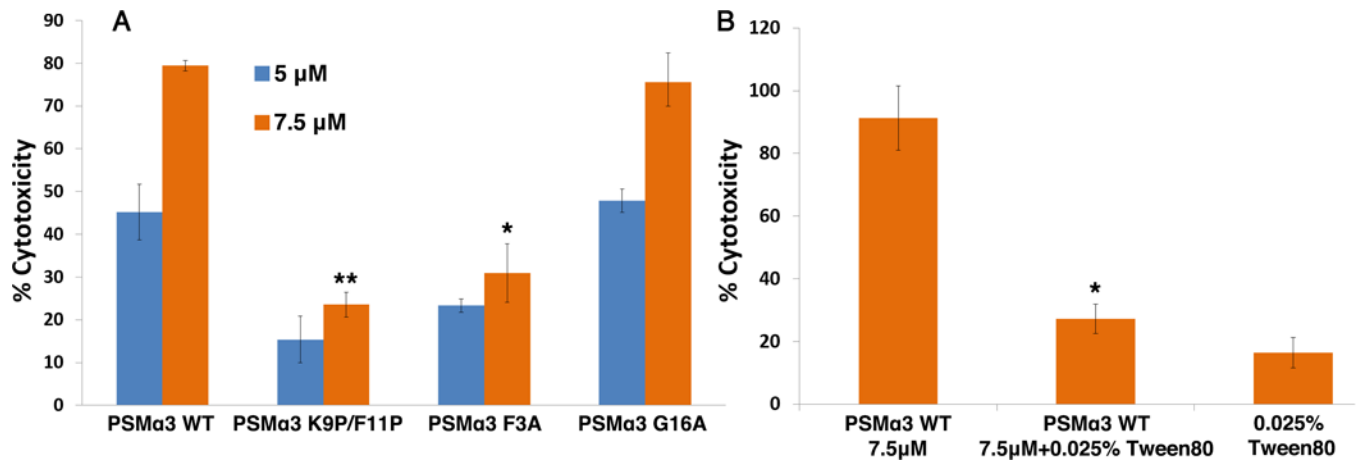


**Fig. 3. PSMα3 toxicity against human T-cells is dependent on its ability to form fibrils.**

(A) PSMα3 is toxic to human T-cells in a dose dependent manner. The F3A mutant and the K9P/F11P double mutant, which do not form fibrils (figs. S8 and S9), exhibited much lower levels of cytotoxicity compared to wild-type PSMα3. G16A, a mutant that is helical and which forms fibrils that bind Thioflavin T, served as a control mutant and proved cytotoxic (figs. S8 and S9). (B) Cytotoxicity of PSMα3 was significantly reduced with the addition of Tween 80, a biocompatible surfactant that diminishes fibrillation (figs. S8 and S10). In both panels, error bars represent the SEM of three replicates. The experiment was performed at least three times on different days. \*  $P < 0.05$  and \*\*  $P < 0.001$  compared to 7.5 μM wild type PSMα3.